BOLETIN DE LA SOCIEDAD ESPAÑOLA DE
Cerámica y Vidrio
www.elsevier.es/bsecv

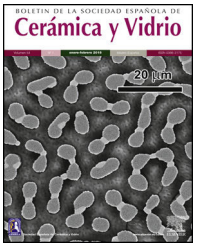

The effect of CuO additive on the mechanical and radiation shielding features of Li_2B4O_7–Pb_2O_3 glass system

K.A. Mahmoud[a,b], M.I. Sayyed[c,d], Abdullah M.S. Alhuthali[e], M.Y. Hanfi[a,b,*]

[a] Ural Federal University, Yekaterinburg, Russia
[b] Nuclear Materials Authority, Maadi, Cairo, Egypt
[c] Department of Nuclear Medicine Research, Institute for Research and Medical Consultations (IRMC), Imam Abdulrahman Bin Faisal University (IAU), Dammam, Saudi Arabia
[d] Department of Physics, Faculty of Science, Isra University,Amman, Jordan
[e] Department of Physics, College of Sciences, Taif University, Taif, Saudi Arabia

ARTICLE INFO

Article history:
Received 14 September 2020
Accepted 19 November 2020
Available online 16 December 2020

Keywords:
Gamma-photons
Mechanical moduli
Shielding properties
Monte Carlo simulation

ABSTRACT

The effect of substitution Pb_2O_3 by CuO content was studied for 75% $Li_2B4O_7 + (25 - x)Pb_2O_3 + xCuO$ glass system where x = 0, 5, 10, 15, 20, and 25 wt%. The mechanical and radiation shielding properties were evaluated for the investigated glass samples. The mechanical properties included Young's, shear, bulk, longitudinal, Poisson ratio, and micro-hardness were computed theoretically based on the packing factor (V_i) and dissociation energy (G_i) of the metal oxides constituting the existing glass samples using the Makishima–Mackenzie model. The obtained results depicted the insertion of CuO enhances the different mechanical parameters up to 20 mol% of the investigated LBPCu glasses. Furthermore, the radiation shielding properties were studied for the investigated LBPCu glass using the Monte Carlo N-particle transport code (MCNP-5) simulation. MCNP-5 was used to detect the simulated linear attenuation coefficient (LAC) and then mass attenuation coefficient (MAC) and other factors based on various gamma-ray sources with energies of 0.24, 0.66, 1.17, 1.33, and 1.40 MeV. The results showed that LAC's highest value decreased from 0.578 to 0.320 cm^{-1} for glasses LBPCu0 and LBPCu25, respectively, at low energy of 0.284 MeV. Moreover, the effective and equivalent atomic numbers (Z_{eff} and Z_{eq}), buildup factor (EBF), and absorption buildup factor (EABF) were evaluated for the investigated LBPCu glass using the BXCOM program. The results revealed that the shielding properties of the investigated glasses improved by the insertion of CuO content.

* *Corresponding author.*
E-mail address: m.nuc2012@gmail.com (M.Y. Hanfi).
https://doi.org/10.1016/j.bsecv.2020.11.005

El efecto del aditivo CuO en las características mecánicas y de protección contra la radiación del sistema de vidrio Li2B4O7 – Pb2O3

Palabras clave:
Gamma-fotones
Módulos mecánicos
Propiedades protectoras
Simulación del Monte Carlo

RESUMEN

Se estudió el efecto de la sustitución de Pb_2O_3 por el contenido de CuO para el 75% de $Li_2B_4O_7 + (25 - x)Pb_2O_3 + xCuO$ sistema de vidrio donde $x = 0$, 5, 10, 15, 20 y 25% en peso. Se evaluaron las propiedades mecánicas y de protección contra la radiación para las muestras de vidrio investigadas. Las propiedades mecánicas incluidas Young, cizallamiento, volumen, longitudinal, relación de Poisson y microdureza se calcularon teóricamente en función del factor de empaquetamiento (V_i) y la energía de disociación (G_i) de los óxidos metálicos que constituyen las muestras de vidrio existentes utilizando el método Makishima-Mackenzie. modelo. Los resultados obtenidos muestran que la inserción de CuO mejora los diferentes parámetros mecánicos hasta en un 20% mol de los vidrios LBPCu investigados. Además, se estudiaron las propiedades de protección contra la radiación para el vidrio LBPCu investigado utilizando la simulación del código de transporte de partículas N de Monte Carlo (MCNP-5). Se utilizó MCNP-5 para detectar el coeficiente de atenuación lineal simulado (LAC) y luego el coeficiente de atenuación de masa (MAC) y otros factores basados en varias fuentes de rayos gamma con energías de 0,24, 0,66, 1,17, 1,33 y 1,40 MeV. Los resultados mostraron que el valor más alto de LAC disminuyó de 0,578 a 0,320 cm^{-1} para los vasos LBPCu0 y LBPCu25, respectivamente, a baja energía de 0,284 MeV. Además, se evaluaron los números atómicos efectivos y equivalentes (Z_{eff} y Z_{eq}), el factor de acumulación (EBF) y el factor de acumulación de absorción (EABF) para el vidrio LBPCu investigado utilizando el programa BXCOM. Los resultados revelaron que las propiedades de protección de los vidrios investigados mejoraron mediante la inserción de contenido de CuO.

Introduction

Ionizing radiation is a form of radiation where the photons have sufficient energy to detach electrons from atoms or molecules. They consist of high energy photons such as X-rays and gamma-rays. Ionizing radiation is common in the medical industry, especially when taking medical exams such as X-ray imaging, CAT scans, PET scans, etc. Besides, it is also used in the fields of agriculture for insect control and in nuclear power to create electricity. Even with the numerous potential benefits that this type of radiation brings, long-term exposure to these photons can cause serious harmful effects. Because of their ability to rip electrons from atoms, high doses may lead to effects such as nausea, skin burns, permanent tissue damage, cancer, and death [1–3].

Three principles are followed to minimize the radiation exposure of workers and patients: time, distance, and shielding. The first two involve limiting the time exposed to radiation and the distance to the source. Although these two principles are essential, it is sometimes necessary to get up close to the radiation source, which is why shielding is needed. Shielding involves any material that is used to protect against radiation. The material can be placed between the person and the source or can be worn to absorb the incoming photons. These materials' goal is to absorb the ionizing radiation's intensity totally or provide safe enough levels [4–6].

There are a few different varieties of materials that are used for shielding. One of these is concrete [7]. Concretes are sturdy materials that offer many desirable qualities, including their ability to form different shapes and low cost. However, they also have some drawbacks, such as their tendency to crack and lack of mobility. Other materials such as alloys are currently being investigated, as their shielding properties are enhanced by mixing different metals [8]. Lead is often used as a shield because of its high density, low cost, and excellent attenuation ability. It can be utilized by itself, mixed into alloys, or doped into another type of material-glasses [9].

Glasses can be modified to enhance their shielding ability, have a low cost, and are transparent, a trait that the other materials do not have. For example, glasses can offer workers the ability to view patients inside a medical facility's radiation room from the outside. They can also be used to make doors in nuclear facilities, create security cameras, and more [10–12]. The heavy metal oxides (HMO) were used as a dopant to improve the glasses' capability to absorb radiation. The metal oxides with a high density have significantly enhanced the effectiveness of glasses against high-energy radiation. There are a few methods used to prepare glass systems. One of the most used methods is called the melt-quenching technique, where the oxides are rapidly heated and are then quenched rapidly [13]. They are often annealed after to remove any stress that might cause the glass to fracture. Other methods are sometimes used, such as chemical vapor deposition (CVD) and the sol–gel process.

The glass system's radiation shielding properties with the composition of $75Li_2B_4O_7–(25 - x)Pb_3O_4–xCuO$, where $x = 0$, 5, 10, 15, 20, and 25 mol%, was investigated. Borate is frequently used as a glass former, an oxide that forms the glass system's backbone because of its hardness and thermal resistance [14]. In the glass system, it can exist as either a tetrahedral BO_4 or a triangular BO_3. CuO acts as a glass modifier in the

borate system, meaning that it does not interconnect with the glass network's backbone but alters it. Previous research has demonstrated that replacing $Li_2B_4O_7$ with CuO increases the amount of BO_3 units in the structure by converting the BO_4 groups. Lead oxide, both of its forms, can act as a glass intermediate, meaning it can act as both a glass former and a glass modifier [15]. Results have shown that about a quarter of the lead oxide acts as a modifier while the rest becomes a network former. The present work novelty lies in the mechanical and gamma-ray shielding features for the evaluated glass network. Based on the Makishima–Mackenzie model, the elastic moduli, Poisson ratio, and micro-hardness were assessed. Besides, the simulation code MCNP-5 and program BXCOM were utilized to evaluate the protection parameter such as linear attenuation coefficient (LAC), transmission factor (TF), and the buildup factors (EBF and EABF).

Materials and methods

Mechanical properties

In the present work, the elastic properties were investigated for a glass network with chemical composition $75Li_2B_4O_7 + (25 - x)Pb_3O_4 + xCuO$ where $x = 0$, 5, 10, 15, 20, 25 mol%. The glass samples were selected from Ref. [15] and coded as LBPCu0–LBPCu25. The chemical concentration in mol% and density were illustrated for the studied glass in Table 1.

The mechanical moduli, such as Young's, shear, bulk, longitudinal, Poisson ratio, and micro-hardness, were computed theoretically based on the packing factor (V_i) and dissociation energy (G_i) of the metal oxides constituting the existing LBPCu0–LBPCu25 glass samples [16,17]. The dissociation energy (G_t) and the packing density of the studied glass were calculated according to Eqs. (1) and (2):

$$G_t\,(\mathrm{kJ\ cm^{-3}}) = \sum_i X_i G_i \tag{1}$$

$$V_t\,(\mathrm{cm^3\,mol^{-1}}) = \frac{\rho}{M}\sum_i X_i V_i \tag{2}$$

The X_i refers to the molar fraction of the ith constituent compound while ρ and M are the density and molecular weight of the studied LBPCu0–LBPCu25 glass samples.

Based on the previously estimated values of the G_t and V_t, the elastic moduli (Young modulus (Y), bulk modulus (B), shear modulus (S), longitudinal modulus (L), Poisson ratio (μ), and microhardness (H)) were computed through the following equations.

$$Y = 2V_tG \tag{3}$$

$$B = 1.2V_tE \tag{4}$$

$$S = \frac{3YB}{(9B - Y)} \tag{5}$$

$$L = B + \frac{3}{4}S \tag{6}$$

$$\mu = \frac{Y}{2S} - 1 \tag{7}$$

$$H = \frac{(1 - 2\mu)}{6(1 + \mu)} \tag{8}$$

Gamma-ray shielding features

Due to the high prices of the pure chemical compounds and the unavailable of the radiation experimental shielding measurements, Monte Carlo N-particle transport code (MCNP-5) was used to simulate the shielding features of the studied LBPCu0–LBPCu25 glass samples. MCNP-5 code is a useful tool supported by continuous-energy nuclear and atomic data libraries. The primary cross-section data sources for the MCNP-5 nuclear database are ENDF, ACTI, ENDL, ACTI, and T-16 files [18]. Due to predict the average track length of the gamma-photons during passing through the studied LBPCu0–LBPCu25 glass samples, an MCNP input file should format. The created input file describes all the simulation tools, such as (the surface card, cell card, material card, importance card, and the source card) [19–21]. The detector assumed an F4 tally to evaluate the emitted photons' average track length inside the studied glasses in the present study. Finally, the prepadeometry was described in Fig. 1.

The shielding factors, such as the linear attenuation coefficient (LAC) and mass attenuation coefficient (MAC) were simulated based on the obtained values of the average track length of the emitted gamma-photons. After that, the simulated MAC and LAC were used to predict other crucial shielding parameters such as the half-value layer ($\Delta_{0.5}$), mean free path (MFP), and transmission factor (TF) [22–24]:

$$\mathrm{LAC\,(cm^{-1})} = \frac{1}{x}\ln\left(\frac{I_o}{I}\right) \tag{9}$$

$$\mu_m = \frac{\mathrm{LAC\,(cm^{-1})}}{\rho\,(\mathrm{g\,cm^{-3}})} \tag{10}$$

$$\mathrm{TF} = \frac{I}{I_o} = \exp^{(-\mathrm{LAC}*x)} \tag{11}$$

$$\mathrm{MFP} = \frac{1}{\mathrm{LAC\,(cm^{-1})}} \tag{12}$$

The I_o, I, x, ρ, w_i, and $(\mu_m)_i$ represent the incoming photon intensity, transmitted photon intensity, glass thickness, glass density, fractional weight, and the ith constituent element's mass attenuation coefficient.

Moreover, a technical program named BXCOM was applied to calculate the effective atomic number (Z_{eff}), equivalent atomic number (Z_{eq}), and the buildup factors (exposure buildup factor (EBF) and energy absorption buildup factor (EABF) for the investigated glasses [25].

Results and discussion

Mechanical properties

Previous works showed that the Pb_2O_3 compounds decomposed to PbO in the furnace under temperature between

Table 1 – The chemical composition and density of the studied glass.

	Chemical composition (mol%)					
	LBPCu0	LBPCu5	LBPCu10	LBPCu15	LBPCu20	LBPCu25
CuO	0.000	05	10	15	20	25
$Li_2B_4O_7$	75	75	75	75	75	75
Pb_3O_4	25	20	15	10	05	0.000
Density ($g\,cm^{-3}$)	4.470	4.300	4.110	3.710	3.530	2.930

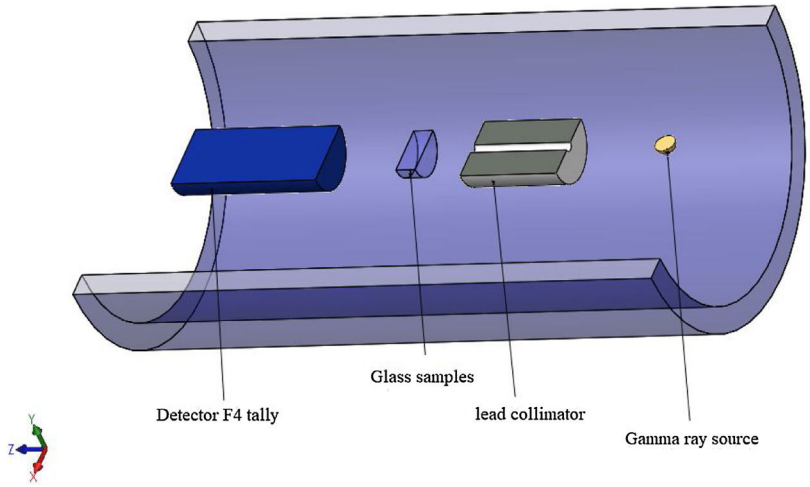

Fig. 1 – The simulation geometry of the present study.

530 and 550 °C while the $Li_2B_4O_7$ was discomposed to Li_2O and B_2O_3, respectively. The elastic quantities, such as elastic moduli (Young, bulk, shear, and longitudinal), Poisson ratio, and micro-hardness, were evaluated for the existing glass samples. According to the Makishima–Mackenzie model, the evaluation was based on the packing factor's calculated values (V_i) and the dissociation energy (G_t) of the metal oxides constituting the studied glass samples. The dependence of V_i and G_t on the CuO content was illustrated in Fig. 2. The calculated values of V_i reach the maximum for the glass sample LBPCu0 without CuO content. After that, the calculated values of the V_i reduced dramatically with the substitution of PbO by CuO. The reason for this reduction is the replacement of PbO with a high packing factor ($V_i = 11.7\,cm^3\,mol^{-1}$) by CuO with a lower packing factor ($V_i = 7.5\,cm^3\,mol^{-1}$). On the other hand, the G_t and V_i have an obverse relationship, where the G_t increased linearly with an increase in the CuO content. The observed trend is due to the replacement of the PbO with lower dissociation energy ($G_t = 25.3\,kJ\,cm^{-3}$) by CuO with higher dissociation energy ($G_i = 59.5\,kJ\,cm^{-3}$) [26].

Additionally, Young's modulus (E) is calculated based on the dissociation energy and packing density (V_t) listed in Table 2 for the existing glass samples. Fig. 3 depicts the variation of the elastic modulus as a function of the CuO concentration, where Young's modulus increased with increasing the CuO up to 20 mol%. After that, the calculated values of Young's

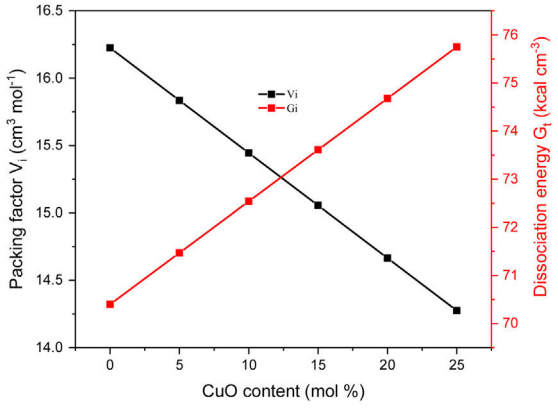

Fig. 2 – Variation of the Packing factor and dissociation energy of the studied LBPCu0–LBPCu25 glass samples.

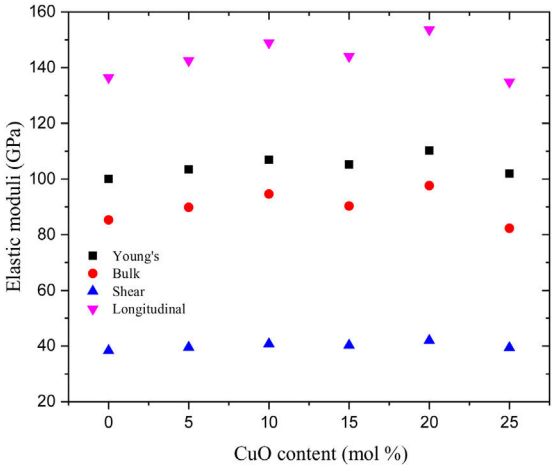

Fig. 3 – Dependence of the elastic moduli on the CuO contents (mol%).

Table 2 – Mechanical properties of the studied glass samples.

Sample code	V_i (mol cm^{-3})	G_t (kJ cm^{-3})	V_t (mol cm^{-3})	E (GPa)	B (GPa)	S (GPa)	μ	H (GPa)	L (GPa)
LBPCu0	15.325	67.20	0.61	93.871	78.676	36.072	0.301	4.782	126.772
LBPCu5	15.115	68.91	0.63	98.547	84.557	37.735	0.306	4.886	134.871
LBPCu10	14.905	70.62	0.64	103.356	90.759	39.443	0.310	4.991	143.350
LBPCu15	14.695	72.33	0.63	102.774	87.618	39.392	0.305	5.134	140.141
LBPCu20	14.485	74.04	0.66	109.182	96.603	41.621	0.312	5.227	152.097
LBPCu25	14.275	75.75	0.60	101.931	82.296	39.399	0.294	5.422	134.828

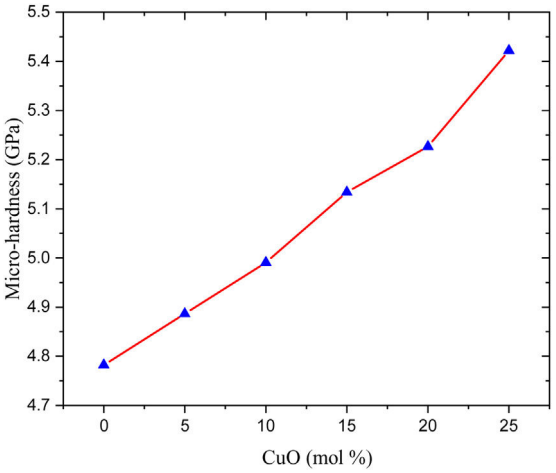

Fig. 4 – Variation of the micro-hardness of the studied LBPCu0–LBPCu25 glass samples as a function of the CuO content (mol%).

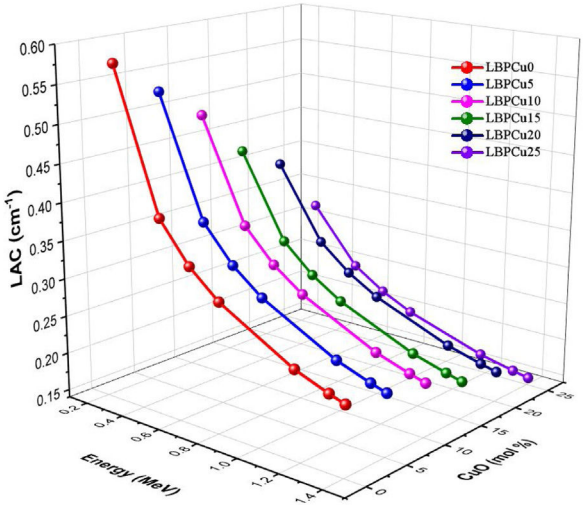

Fig. 5 – Variation of the linear attenuation coefficient LAC (cm^{-1}) versus the incident gamma photon energy at different concentrations of CuO content.

dropped suddenly at CuO content 25 mol%. The reason for dropping the elastic modulus (*E*) at a high concentration of CuO (25 mol% for the glass LBPCu25) is the decrease of the V_t of the studied glasses where $E\alpha V_t$. Fig. 3 also depicts the bulk, shear, and longitudinal moduli variation versus the CuO insertion ratio. The calculated quantities of bulk, shear, and longitudinal moduli follow Young's modulus in quite the same order. The computed values of Young's, bulk, shear, and longitudinal moduli were changed in the range between 93.87–101, 78.67–82.29, 36.07–39.39, and 126.77–134.82 GPa, respectively, for the studied LBPCu0–LBPCu25 glass samples.

As mentioned earlier, the Poisson ratio was also calculated according to Eq. (7), where it is directly proportional to linearly increase with an increase in the existing glass samples' V_t. Table 2 lists the Poisson ratio's calculated values, where it also follows Young's modulus in quite the same order. It is increased from 0.27 to 0.29, with an increase in the CuO insertion ratio between 0 and 20 mol%. After that, the Poisson ratio dropped to 0.294 for the CuO insertion ratio of 25 mol%. The detected drop is due to the sudden decrease in the V_i and V_t of the studied LBPCu25 glass sample.

Hardness is a mechanical property used to check the material's ability to resist the incoming loading and is divided into two types: micro-hardness and macro-hardness. The glass samples usually small and with a thinner thickness. Thus, the micro-hardness (*H*) is more important to study in the present work. The data presented in Fig. 4 and listed in Table 2, the studied glass samples' micro-hardness, increases gradually from 4.782 to 5.422 Gpa when the CuO ratio varied in the range between 0 and 25 mol%, respectively.

A comparison was performed between the elastic moduli calculated for the present glass system and some previously measured elastic moduli for borate glasses containing CuO and PbO compounds to confirm the theoretical model's results for the studied LBPCu0–LBPCu25 glass samples presented in Table 3. It is clear that the calculated elastic moduli are comparable to those measured for borate glass containing CuO and lead reported by Refs. [27] and [28], respectively. It is higher than the elastic moduli of the measured for the borate glasses containing PbO [29,30].

Ionizing radiation shielding capacity

Monte Carlo N-particle transport code (MCNP-5) was used to detect the investigated glasses' simulated linear attenuation coefficient (LAC). Fig. 5 illustrates that the incident gamma photon energy, and the chemical composition is the two main factors affecting the LAC. First, the dependence of the LAC on the incident gamma photon energy. The investigated LBPCu glasses' results depict that the LAC decrease with an increase in the incident gamma photon energy. At low energy 0.284 MeV, the LAC has the highest values. The highest LAC diminished from 0.578 to 0.320 cm^{-1} for glasses LBPCU0 and LBPCu25, respectively. Subsequently, the simulated LAC values progressively decreased with the increase in the

Table 3 – Comparison between experimental elastic moduli of previously prepared borate glasses and the calculated model in the present work.

Sample code	Composition (mol fraction)	Density (g cm^{-3})	E (GPa)	B (GPa)	S (GPa)	μ	H (GPa)	L (GPa)
LBPCu0	$0.75Li_2B_4O_7$, $0.25Pb_2O_3$	4.470	93.871	78.676	36.072	0.301	4.782	126.772
LBPCu20	$0.75Li_2B_4O_7$, $0.05Pb_2O_3$, 0.2CuO	3.350	109.182	96.603	41.621	0.312	5.227	152.097
LBPCu25	$0.75Li_2B_4O_7$, 0.25CuO	2.930	101.931	82.296	39.399	0.294	5.422	134.828
BCCu0.05 [27]	$0.6B_2O_3$, 0.35CaO, 0.05CuO	2.7442	96.87	76.84	37.55	0.2889	5.259	126.90
BCCu0.1 [27]	$0.6B_2O_3$, 0.3 CaO, 0.1CuO	2.897	112.60	84.75	44.03	0.278	6.5	143.46
BCCu0.15 [27]	$0.6B_2O_3$, 0.25CaO, 0.15CuO	3.0963	131.23	91.67	52.02	0.2614	8.273	161.02
BCCu0.2 [27]	$0.6B_2O_3$, 0.2 CaO, 0.2CuO	3.2991	144.96	100.47	57.54	0.2595	9.224	177.20
25 PbO [30]	$0.2Na_2O$, $0.55B_2O_3$, 0.25PbO	3.675	60.7	42.2	24.1	0.260	–	74.3
LBPb20 [29]	$0.2Li_2O$, $0.6B_2O_3$, 0.2PbO	–	75	49	29	0.27	–	94
CL4 [28]	$0.15Li_2O$, 0.2PbO, $0.65B_2O_3$	3.76	70.79	51.52	27.85	–	–	88

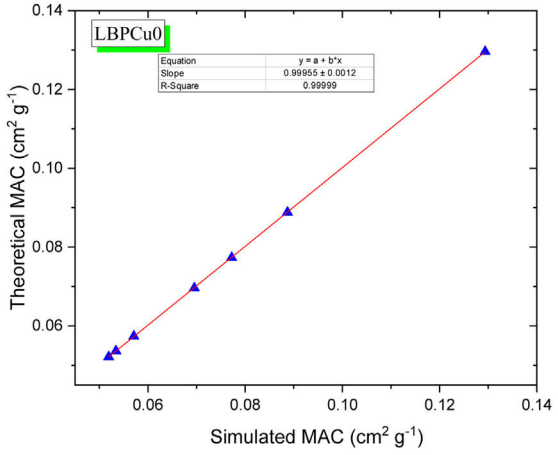

Fig. 6 – The relation between the theoretical and simulated MAC for the glass sample LBPCu0 for an example.

incident energy of gamma photons. This is because the Compton scattering cross-section is inversely proportional to the incident gamma photon energy. At energy of 1.406 MeV, the lowest LAC was observed and decreased from 0.232 to 0.149 cm^{-1} for glasses LBPCu0 and LBPCu25, respectively.

The other factor is the chemical composition of the LBPCu glasses. The replacement of Pb_3O_4 content by CuO on the existing glass decreases the molecular weight of LBPCu glasses. Therefore, Z_{eff} decreases moderately by reducing the molecular weight of the LBPCu glasses. The maximum value of LAC was attached before the CuO content was added to the selected glass, while the lowest values were obtained for the LBPCu25 glass with 25 mol% CuO. For the LBPCu0 glass sample (as an example), the LAC varied in a decreasing trend from 0.578 to 0.232 cm^{-1}, while it is diminished from 0.32 to 0.149 cm^{-1} for the LBPCu20 glass sample at gamma-photon energy range between 0.284 and 1.406 MeV. The obtained results illustrated that the LAC decrease with increasing the CuO content to Pb_3O_4 glasses. The LAC reduction is due to CS's cross-section, which is proportional directly to Z_{eff} ($\sigma_{com} \alpha Z_{eff}$).

The mass attenuation coefficient (MAC) was calculated theoretically using XCOM and correlated with MAC simulated based on LAC data. The strong correlation between theoretical and simulated MAC for selected LBPCu0 glass is presented in Fig. 6. The difference (%) between simulated and hypothetical was less than 2% for LBPCu glasses, where it was calculated according to Eq. (13).

$$\text{Diff}\,(\%) = \frac{\left[(\mu_m)_{\text{mcnp}} - (\mu_m)_{\text{xcom}}\right]}{(\mu_m)_{\text{mcnp}}} \times 100 \quad (13)$$

Fig. 7 exhibits the studied glass's TF variation with the thickness of the investigated glass at stationary gamma photon energies (0.284, 0.662, 1.173, and 1.406 MeV). First, the reliance of the TF studied on the incoming gamma-photon energy. The TF was observed to increase with increasing the incident gamma-photon energy. At low energy 0.284 MeV, the little values of TF were detected for the LBPCu0 glass sample and diminish from 56.08 to 5.50%, while the highest TF decreased from 72.58 to 20.15% for the LBPCu25 glass sample. Additionally, at gamma-photon energy 1.406 MeV, the TF ranged between 79.28–31.33 and 86.09–47.29% for LBPCu0 and LBPCu25, respectively. As a result of the increasing incident photon energy, the incoming photons photon's penetration power increases, and the wavelength of gamma-photon will decrease ($E = hc/\lambda$). Consequently, the number of interactions inside the LBPCu glasses decreased, and the transmission of photons increased.

Second, the thickness of the LBPCu-glass samples affected the TF of the incident photons. For LBPCu25 glass, the TF at low energy (0.284 MeV) decreases from 72.58 to 20.15%, increasing the glass thickness from 1 to 5 cm, respectively. With expanding the glass thickness, the incident photon takes a long time to penetrate the glass thickness. Thus, photon interactions will increase inside the glass, and the transmitted photons will decrease.

Fig. 8 displays the variation of the MFP with the selected energy range for the investigated LBPCu0-LBPCu25 glass samples. Also, in this figure we included the MFP for the previously fabricated borax glass [31] and commercial shielding glass RS-253-G18. The MFP of the studied LBPCu glasses is increased with the increasing incident photon gamma energy. The maximum value of MFP was observed for the LBPCu25 glass sample, while the minimum value was obtained for the LBPCu0 glass. LBPCu glasses' MFP values are even lower than RS-253-G18 and Borax 40% as an appropriate high-density shielding glass. This illustrates that the average distance between two successive interactions of the incident gamma photons in the investigated LBPCu glasses is short. This is due to the low weight fraction of Cu in the investigated glasses.

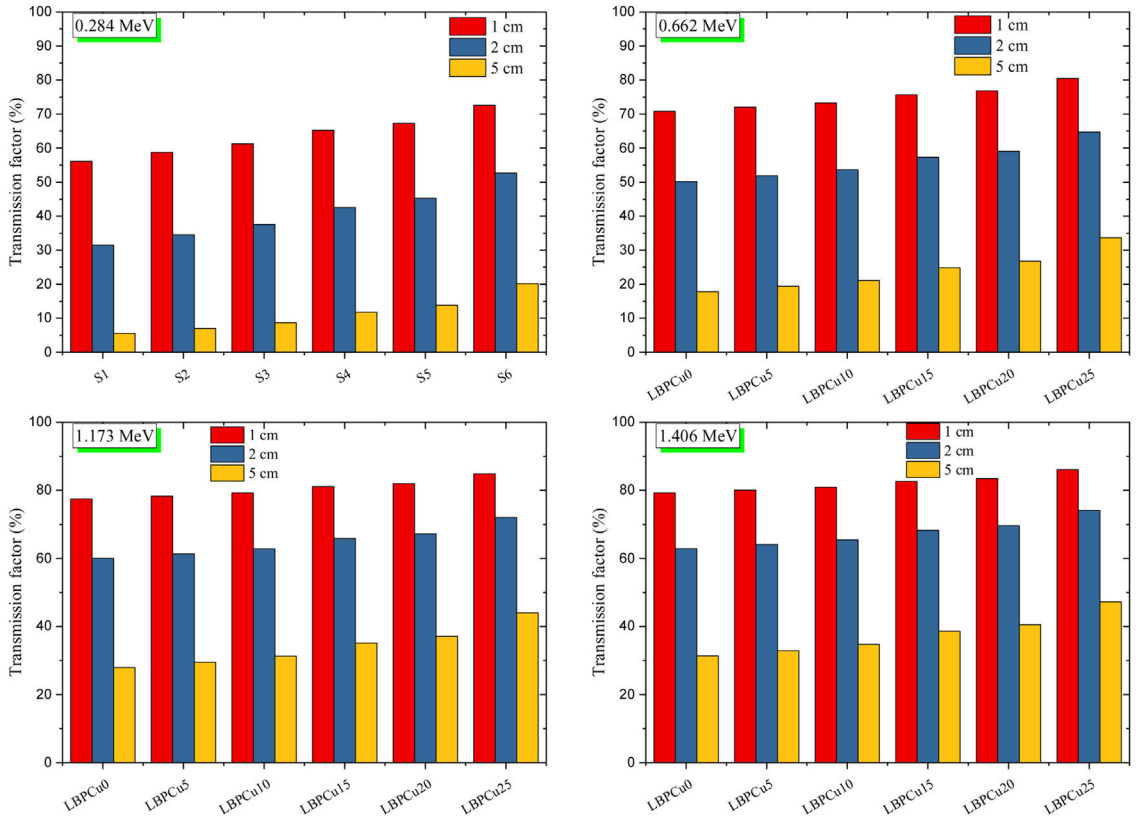

Fig. 7 – Variation of the transmission factor of the investigated glass samples versus the glass thickness at fixed gamma-ray energies.

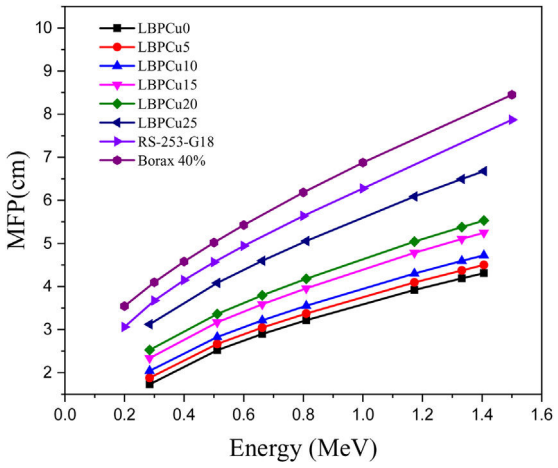

Fig. 8 – Comparison between the MFP of the investigated glass, commercial glass sample RS-253-G18, and some similar previously fabricated glass samples.

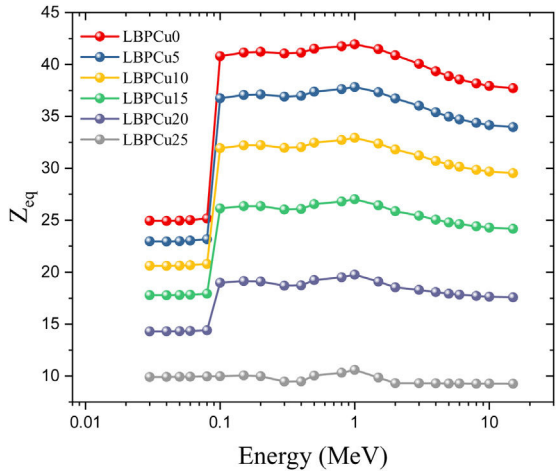

Fig. 9 – Dependence of the equivalent atomic number as a function of gamma-photon energies.

Based on the Compton scattering mass attenuation coefficient (MAC_{CS}) of the constituent elements in the glass network, the Z_{eq} values were calculated in the gamma-photon energy range between 0.015 and 15 MeV and presented in Fig. 9. The values of the Z_{eq} showed a dependence on the photon energy, where the lowest Z_{eq} was detected in the PE energies range between 0.015 and 0.1 MeV. At gamma-energies above 0.1 MeV, where the CS interaction is prevalent, the Z_{eq} values increase progressively. Above 1 MeV, the Z_{eq} decreases gradually due to the increase in PP interactions.

The buildup factors are usually used to describe the accumulation of gamma-photons. The buildup factors are divided into exposure buildup factor (EBF), which predicts the number of gamma-photons accumulated in the air after passing the material, and energy absorption buildup factor (EABF), which

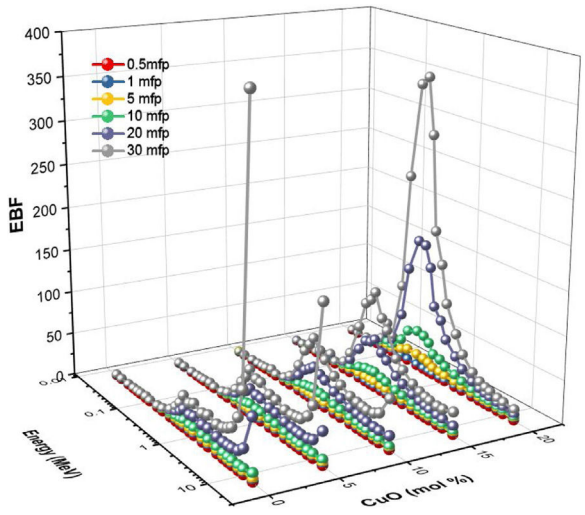

Fig. 10 – The dependence of the exposure buildup factor (EBF) versus the incoming gamma photon energy and penetration depth.

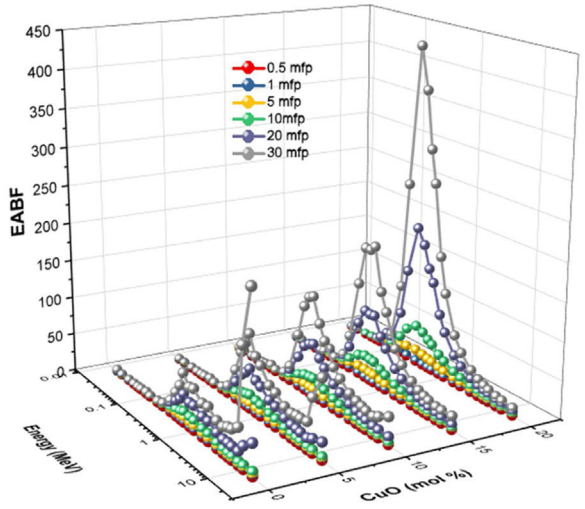

Fig. 11 – The dependence of the energy absorption buildup factor (EABF) versus the incoming gamma photon energy and penetration depth.

indicates the number of photons heaped up inside the studied glass thickness. The program BXCOM was used to calculate EBF and EABF for gamma-photon energies between 0.015 and 15 MeV. Figs. 10 and 11 depict the EBF and EABF values' dependence on three parameters (incoming gamma-photon energy, samples penetration depth in the unit of mfp, and the glass composition). Firstly, the computed values of EBF and EABF possess lower vales at low gamma-photon energies, where the photo-electric interaction (PP) interaction removes almost the incident gamma-photons. After that, the number of heading up photons increases gradually with the increasing Compton scattering interaction. Compton scattering interaction removes only a small part of the incident photon energy during the interaction. The scattered photon accumulated inside the studied glass thickness with the rest of the incident photon energy. For the gamma-photon energies higher than 2 MeV, the pair production (PP) began to dominate. Thus, the number of EBF and EABF values gradually decreased with increasing the incident gamma photons. It is observed that at high energies (higher than 8 MeV), glass samples LBPCu0 and LBPCu5 have a rapid increase in the EBF and EABF values, and this trend decreased gradually with decrease Pb_2O_3 contents in the studied glass samples. It is also observed that the highest values of the EBF and EABF achieved at high energies (energy >8 MeV) for glass samples LBPCu0 and LBPCu5 which contain 20 and 15 mol% of Pb_3O_4, respectively. Secondly, the computed values of EBF and EABF were observed to increase systematically with an increase in the penetration depth (PD) up to 20 mfp. The gamma photons spent a more extended period to penetrate the thicker thickness, leading to more photons accumulation. It is observed that the lowest values of the EBF and EABF achieved at little PD (PD = 0.5 mfp) while the highest values of EBF and EABF were obtained at high PD (PD = 40 mfp). Finally, the variation of EBF and EABF values versus the chemical composition is illustrated in Figs. 10 and 11. The calculated values of the EBF and EABF increased with the replacement of Pb_3O_4 with the CuO content, where the lowest and highest buildup factors were obtained at 0 and 20 mol% CuO. As the CuO content ratio increases, the computed values of the EABF increased while the EBF values decreased. Thus, the replacement of Pb_3O_4 by CuO leads to accumulating the incoming photons in the studied glass.

Conclusion

The mechanical and radiation protection characteristics were investigated for the LBPCu glass network. Firstly, the assumptions of Makishima–Mackenzie's theory were used to calculate the elastic moduli. Thus, the packing factor (V_i) and dissociation energy (G_t) were calculated for the mentioned glass system. The V_i and G_i's estimated values were ranged between 15.32–14.27 $cm^3\ mol^{-1}$ and 33.85–54.22 $kJ\ cm^{-3}$, respectively, with the increase of CuO insertion ratio between 0 and 25 wt%. Young's modulus was enhanced and increased between 93.87 and 101.93 GPa, increasing the CuO insertion ratio between 0 and 25 wt%. The rest of the mechanical moduli were observed to follow the trend of Young's modulus. The protection ability against gamma-ray was evaluated utilizing the MCNP-5 code for photons with energy ranging between 0.284 and 0.320 cm^{-1} for the studied glass sample LBPCu0 and LBPCu25. The simulated results showed that the substitution of Pb_2O_3 with CuO diminished the shielding features of the LBPCu glass system. The RPE of the studied glasses follows the LAC trend (decreased with increasing the incident gamma energy). The TF and $\Delta_{0.5}$ has opposite directions with the LAC, where the TF increased with increasing the incident gamma-photon energy. The buildup factors were calculated using the BXCOM program. The computed results showed enhancement of the EBF and EABF values with increasing the insertion ratio of CuO in the glass network.

Acknowledgement

We would like to thank Taif University Researchers Supporting Project number (TURSP-2020/226), Taif University, Taif, Saudi Arabia for financial support.

REFERENCES

[1] Y. Al-Hadeethi, M.I. Sayyed, Y.S. Rammah, Fabrication, optical, structural and gamma radiation shielding characterizations of GeO_2–PbO–Al_2O_3–CaO glasses, Ceram. Int. 46 (2020) 2055–2062.
[2] L.S. Dartnell, Ionizing radiation and life, Astrobiology 11 (2011) 551–582.
[3] J.E. Martin, Physics for Radiation Protection: A Handbook, John Wiley Sons, 2006.
[4] H.C. Manjunatha, K.V. Sathish, L. Seenappa, G. Damodara, S. Alfred Cecil Raj, A study of X-ray, gamma and neutron shielding parameters in Si-alloys, Radiat. Phys. Chem. 165 (2019) 108414.
[5] S.S. Obaid, M.I. Sayyed, D.K. Gaikwad, H.O. Tekin, Y. Elmahroug, P.P. Pawar, Photon attenuation coefficients of different rock samples using MCNPX, Geant4 simulation codes and experimental results: a comparison study, Radiat. Eff. Def. Solids 173 (2018) 900–914, http://dx.doi.org/10.1080/10420150.2018.1505890.
[6] B. Raza, K.M. Alireza, S. Sayed Pezhman, A. Bakhtair, S. Mojtaba, Determination of gamma-ray shielding properties for silicate glasses containing Bi_2O_3, J. Non-Cryst. Solids 479 (2018) 62–71.
[7] R.S.M. Rashid, S.S. Mohammed, N.M. Azreen, Y.L. Voo, M. Haniza, A.A. Shukri, S.Y. Mohd, Effect of elevated temperature to radiation shielding of ultra-high performance concrete with silica sand or magnetite, Construct. Build. Mater. 262 (2020) 120567.
[8] A. Bünyamin, High alloyed new stainless steel shielding material for gamma and fast neutron radiation, Nucl. Eng. Technol. 52 (2020) 647–653.
[9] Y. Al-Hadeethi, M.I. Sayyed, M. Hiba, L. Rimondin, X-ray photons attenuation characteristics for two tellurite-based glass systems at dental diagnostic energies, Ceram. Int. 46 (2020) 251–257.
[10] A. Aşkın, Gamma and neutron shielding characterizations of the Ag_2O–V_2O_5–MoO_3–TeO_2 quaternary tellurite glass system with the Geant4 simulation toolkit and Phy-X software, Ceram. Int. 46 (2020) 6046–6051.
[11] A. Aşkın, Evaluation of the radiation shielding capabilities of the $Na_2B_4O_7$–SiO_2–MoO_3–Dy_2O_3 glass quaternary using Geant4 simulation code and Phy-X/PSD database, Ceram. Int. 46 (2020) 9096–9102.
[12] V.P. Singh, N.M. Badiger, J. Kaewkhao, Radiation shielding competence of silicate and borate heavy metal oxide glasses: comparative study, J. Non-Cryst. Solids 404 (167AD) (2014).
[13] M.I. Sayyed, A.A. Ali, M.H.A. Mhareb, K.A. Mahmoud, K.M. Kaky, Baki, M.A. Mahdi, Novel tellurite glass $(60-x)TeO_2$–$10GeO_2$–20ZnO–10BaO–xBi_2O_3 for radiation shielding, J. Alloy. Compd. 844 (2020) 155668, http://dx.doi.org/10.1016/j.jallcom.2020.155668.
[14] A.S. Abouhaswa, R. El-Mallawany, Y.S. Rammah, Direct influence of La on structure, optical and gamma-ray shielding properties of lead borate glasses, Radiat. Phys. Chem. 177 (2020) 109085.
[15] I. Kashif, A. Abd El-ghany, A. Abd El-Maboud, M.A. Elsherbiny, A.M. Sanad, IR, density and DTA studies the effect of replacing Pb_3O_4 by CuO in pseudo-binary $Li_2B_4O_7$–Pb_3O_4 glass system, J. Alloy. Compound. 503 (2010) 384–388.
[16] A. Makishima, J.D. Mackenzie, Direct calculation of Young's modulus of glass, J. Non-Cryst. Solids 12 (1973) 35–45.
[17] A. Makishima, J.D. Mackenzie, Calculation of Bulks modulus, Shear modulus and Piosson's ratio of glass, J. Non-Cryst. Solids 17 (1975) 147–157.
[18] J. Briesmeister, MCNP – A General Monte Carlo Code for Neutron and Photon Transport. Report LA13709-M. Version 4C, National Laboratory, Los Alamos, 2000.
[19] A.S. Abouhaswa, M.I. Sayyed, K.A. Mahmoud, Y. Al-Hadeethi, Direct influence of mercury oxide on structural, optical and shielding properties of a new borate glass system, Ceram. Int. (2020), http://dx.doi.org/10.1016/j.ceramint.2020.04.112.
[20] R. Divina, K. Marimuthu, K.A. Mahmoud, M.I. Sayyed, Physical and structural effect of modifiers on dysprosium ions incorporated boro-tellurite glasses for radiation shielding purposes, Ceram. Int. 46 (2020) 17929–17937, http://dx.doi.org/10.1016/j.ceramint.2020.04.102.
[21] K.A. Mahmoud, E. Lacomme, M.I. Sayyed, Ö.F. Özpolat, O.L. Tashlykov, Investigation of the gamma ray shielding properties for polyvinyl chloride reinforced with chalcocite and hematite minerals, Heliyon 6 (2020) e03560.
[22] M. Dong, X. Xue, A. Kumar, H. Yang, M.I. Sayyed, S. Liu, E. Bu, A novel method of utilization of hot dip galvanizing slag using the heat waste from itself for protection from radiation, J. Hazard. Mater. 344 (2018) 602–614.
[23] M. Dong, X. Xue, H. Yang, D. Liu, C. Wang, Z. Li, Comprehensive utilization of vanadium slag: as gamma ray shielding material, J. Hazard. Mater. 318 (2016) 751–757.
[24] R. El-mallawany, M.I. Sayyed, M.G. Dong, Y.S. Rammah, Simulation of radiation shielding properties of glasses contain PbO, Radiat. Phys. Chem. 151 (2018) 239–252, http://dx.doi.org/10.1016/j.radphyschem.2018.06.035.
[25] Ö. Eyecioğlu, A.M. El-Khayatt, Y. Karabul, M. Çağlar, O. Toker, O. İçelli, BXCOM: a software for computation of radiation sensing, Radiat. Eff. Def. Solids 174 (2019) 506–518, http://dx.doi.org/10.1080/10420150.2019.1606811.
[26] S. Inaba, S. Fujino, K. Morinaga, Young's modulus and compositional parameters of oxide glasses, J. Am. Ceram. Soc. 82 (1999) 3501–3507.
[27] C. Subashini, R.E. Pavai, J. Subashini, L. Balu, P. Eswaran, R. Ravisankar, Investigation of structural and ultrasonic properties of ternary borate glass specimen, Mater. Today Proceed. (2020), http://dx.doi.org/10.1016/j.matpr.2020.08.347.
[28] V.C. Veeranna Gowda, R.V. Anavekar, K.J. Rao, Elastic properties of fast ion conducting lithium based borate glasses, J. Non-Cryst. Solids 351 (2005) 3421–3429.
[29] V.C. Veeranna Gowda, R.V. Anavekar, Elastic Properties and Spectroscopic Studies of Lithium Lead Borate Glasses, Ionics 10 (n.d.) 103–108.
[30] M.S. Gaafar, I.S. Mahmoud, Structural investigation and interpretation of some alkali lead borate glasses as radiation shielding materials, J. Aust. Ceram. Soc. 55 (2019) 865–872.
[31] N.Y. Yorgun, E. Kavaz, H.O. Tekin, M.I. Sayyed, Ö.F. Özdemir, Borax effect on gamma and neutron shielding features of lithium borate glasses: an experimental and Monte Carlo studies, Mater. Res. Express 6 (2019) 115217, http://dx.doi.org/10.1088/2053-1591/ab4fcc.